RSC Advances

ROYAL SOCIETY OF CHEMISTRY

www.rsc.org/advances

Table of contents: textual abstract

A bio-derived silk-fibroin film doped with a luminescent dye and its application as luminescent down-shifting layer in organic solar cells.

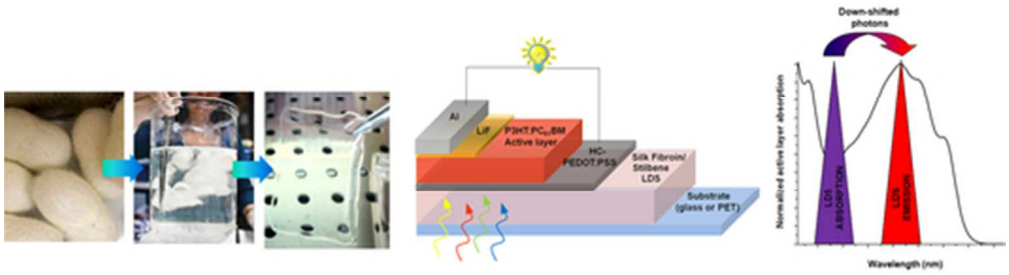

22x6mm (600 x 600 DPI)

Journal Name

RSCPublishing

ARTICLE

Integration of a silk fibroin based film as luminescent down-shifting layer in ITO-free organic solar cells

Cite this: DOI: 10.1039/x0xx00000x

Received ooth January 2012,
Accepted ooth January 2012

DOI: 10.1039/x0xx00000x

www.rsc.org/

Mario Prosa,[a] Anna Sagnella,[b] Tamara Posati,[c] Marta Tessarolo,[a] Margherita Bolognesi,[c] Susanna Cavallini,[a] Stefano Toffanin,[a] Valentina Benfenati,*[b] Mirko Seri,*[b] Giampiero Ruani,[a] Michele Muccini[a] and Roberto Zamboni[b]

We report here a study on the integration of the silk fibroin (SF) protein in organic solar cells. The intrinsic low toxicity, natural availability, biodegradability, water processing, good film forming properties and capability to be doped with functional molecules of SF biopolymer inspired us to integrate it as transparent and inert or functional bottom layer in organic solar cells. Water stable, optically transparent, smooth and homogeneous SF thin films (thickness ~ 400 nm) were successfully prepared on glass and characterized. Then ITO-free bulk heterojunction (BHJ) solar cells employing $P_3HT:PC_{61}BM$ as standard active layer and a highly conductive PEDOT:PSS formulation as semi-transparent anode were deposited over the SF films. As a result, the power conversion efficiency (PCE) of all silk-integrated BHJ solar cells was comparable to the references on bare glass. The ability of SF to act as host matrix for functional moieties was exploited to give to the SF layer the functionality of Luminescent Down-shifting film (LDS), as confirmed by the spectral response measurements, by using a water soluble stilbene derivative (Stb). The photovoltaic performance of all SF-based devices resulted significantly stable over time, overcoming that of the ITO-based reference cells after 70 days. Finally, flexible SF-integrated ITO-free solar cells were successfully fabricated on PET substrates.

1. Introduction

Nowadays, research has to respond to the growing need for novel functional materials to be employed in the field of organic electronics, which is rapidly developing towards increasingly performing devices. Indeed, organic materials represent the future of clean energy conversion and storage, allowing the fabrication of low cost, solution processable, large area and flexible opto-electronic devices [1]. Together with this, the need for tailorable, biocompatible and eco-friendly materials to address the urgent problem of the environmental sustainability of the new organic-based technologies is another important scientific challenge [2]. In sight of this, many researches aimed at identifying compounds of natural origin and establishing economically efficient routes for their integration in high-technology manufacturing pathways. Biopolymers, *i.e.* materials produced and/or modified by living organisms, have suitable features to generate green and eco-friendly organic electronics. They combine properties as: i) biological synthesis, ii) reduced toxicity, iii) biodegradability, iv) wide availability, v) water based processing and vi) good film-forming properties, required for their integration in optoelectronic devices [3]. For example, several biopolymers such as cellulose [4], poly-L-lactic acid (PLA) [5] and glucose [6], have been successfully used as substrates for optoelectronic devices such as organic light emitting diodes (OLEDs), organic field effect transistors (OFETs) and organic photovoltaics (OPVs). Among biomaterials, the silk fibroin (SF) natural protein, extracted from *Bombyx mori* cocoon, represents a very promising alternative for green bio-derived optoelectronic devices [7]. Of particular interest is the SF poly-functionality, arising from its outstanding physical, chemical and mechanical properties. In fact SF can be easily processed from eco-friendly aqueous solution in different forms including fibers, capsules, particles, foams, gels and films [8]. Moreover, the SF ability to host functional compounds such as nanoparticles (NPs) and/or optically active molecules, [9] allows to tailor the SF properties and confer to it additional functionalities. Thanks to these exceptional characteristics, pure SF has been already employed for the fabrication of optical elements (namely refractive and diffractive lenses, gratings, photonic crystals, optical fibers and microfluidic circuits) [10] and of supporting substrates for

implantable bio-integrated electronics [11], while doped SF has been demonstrated to be suitable for the fabrication of electro-optically active films (solar concentrators, scattering layers, lasing films) [12, 9].

Besides the importance of these studies, at present the possibility to integrate SF films in organic solar cells to obtain biocompatible devices and/or improved OPV performance has never been explored. In this work, therefore, we report a novel study on silk-integrated BHJ devices. Water resistant, optically transparent, smooth and homogeneous SF thin films (thickness ~ 400 nm) on glass or flexible polyethylene terephtalate (PET), were prepared and characterized. Then, ITO-free BHJ solar cells employing poly(3-hexyl)thiophene and phenyl-C61-butyric acid methyl ester (P3HT:$PC_{61}BM$) as standard active layer and a highly conductive poly(3,4-ethylenedioxythiophene):poly(styrenesulfonate) (HC-PEDOT:PSS) formulation as semi-transparent anode [13] were fabricated on the top of the SF layer, to obtain OPV devices with performance comparable to that of the analogous reference systems on bare glass (or PET) supports. The possibility to obtain flexible devices on PET/SF film substrates was demonstrated by comparing the performance of the silk integrated devices and reference devices on PET, before and after bending cycles. This study also represents a promising step towards the obtainment of flexible devices supported on free standing silk films.

To prove the potential multifunctionality of the SF film as bottom layer in OPVs, we aimed to convert it into a luminescent down-shifting layer (LDS). An ideal LDS layer enhances the overall photocurrent of the solar cell by widening its spectral response in the range of absorption of the LDS [14]. To this aim, we doped thin SF films with a commercial and water soluble derivative of stilbene (Stb), from the class of azo-dyes. Stilbene dyes are phytochemicals that are well known since decades for their high emission quantum yields (QY) [15]. Moreover, in our previous work [12b], Stb was already demonstrated to be easily dispersed in SF without altering the host film properties and still functioning as highly luminescent dye. Thus, Stb-doped SF films were applied as LDS in ITO-free BHJ solar cells. The effect of the LDS layer on the photovoltaic response of the device was clearly detectable by measuring the spectral response, even though not being appreciable by the I-V curve measurements under standard illumination.

Of note, these encouraging results were also accompanied by an improved chemical-physical stability and shelf life of the silk-based devices, compared to the reference ones. The herein reported results pave the way for more efficient, bio-compatible, fully solution processable, inexpensive and flexible silk-based ITO-free solar cells.

2. Experimental

2.1 Materials

All reagents, PEDOT:PSS (Clevios P VP Al 4083, Heraeus), highly conductive PEDOT:PSS (Clevios PH 500,Heraeus), poly(3-hexyl-thiophene) (P3HT, Rieke Metals), Phenyl-C61-butyric acid methyl ester ($PC_{61}BM$, American Dye Source), Triton X-100 surfactant (Sigma Aldrich), Sodium carbonate (Na_2CO_3, Sigma Aldrich), Lithium bromide (LiBr, Sigma Aldrich), Dimethylsulfoxide (DMSO, Sigma Aldrich), Stilbene 420 (Exciton), conductive silver paste (RS components) and other anhydrous solvents (Sigma Aldrich) were purchased from commercial sources and used without further purification. All PEDOT:PSS-based solutions were used after previous filtration with a microfilter (pore size 0.45 μm).

2.2 Extraction of silk fibroin

Silk fibroin solution was prepared from *Bombyx mori* silkworm cocoons according to the reported procedures [16]. The cocoons were degummed in boiling 0.02 M Na_2CO_3 solution for 45 min. The extracted fibroin was then rinsed three times in Milli-Q water and dissolved in a 9.3 M LiBr solution at 60 °C for 6 h. Subsequently, the SF solution was dialyzed (dialysis membranes, MWCO3500) against distilled water for 48 h and centrifuged three times at 4000 rpm for 20 minutes to obtain pure regenerated SF water-solution (ca. 6-7 wt/vol %). The SF water-solution was stored at 4°C.

2.3 Silk fibroin film preparation

Glass or PET substrates were cleaned in sequential sonicating baths (for 15 min) of deionized water, acetone and isopropanol. After the final sonication step, substrates were dried with a stream of Argon gas and then placed in an oxygen plasma chamber for 10 min. Water insoluble pure SF films were obtained by doping the pristine SF solution with DMSO (2.5% v/v). Stb-doped insoluble SF films were analogously obtained by mixing 3wt %, 5wt % or 7wt % of Stilbene 420 to the SF/DMSO solution.

Next, the SF/DMSO or the Stb/SF/DMSO mixture was spun cast with a two-steps procedure (first at 1000 rpm for 180 seconds and then at 3000 for 20 seconds) on the glass (or PET) substrates obtaining ~ 400 nm thick layers.

For simplicity, the SF/DMSO and Stb/SF/DMSO will be respectively coded as “SF” and “Stb:SF”.

2.4 OPV Device fabrication and characterization

For the fabrication of standard ITO-based devices, a solution of PEDOT:PSS (Clevios P VP Al 4083, Heraeus) was spin coated onto previously cleaned and UV-ozone treated ITO-coated glasses (Thickness = 150 nm, Rs ~ 10 Ω/sq, ITO roughness RMS <1 nm) and subsequently annealed at 150°C for 15 minutes in air. The thickness of PEDOT:PSS layer resulted to be ~ 30 nm.

Differently, for the fabrication of ITO-free devices, the solution of highly conductive PEDOT:PSS (Clevios PH 500, Heraeus) was doped with i) 5% (v/v) of DMSO and ii) 1% (v/v) Triton X-100 surfactant to improve the conductivity [17] and the thin film quality [18], respectively, of the PEDOT:PSS layer. The resulting solution was stirred at room temperature for 1 day and successively spin coated on glass (bare or SF-coated glass) or PET and annealed at 120°C for 20 minutes in air. After the

deposition of the doped highly-conductive PEDOT:PSS, silver paste was deposited on a small area of the polymer anode for the external circuit contact.
For simplicity, the doped highly-conductive PEDOT:PSS is coded in this paper as HC-PEDOT:PSS.
The active blend was formulated by dissolving P3HT and $PC_{61}BM$ (1:1 wt/wt ratio) in anhydrous chlorobenzene:orthodichlorobenzene solution (CB:ODCB, 1:1 v/v) with a total concentration of 60 mg/ml. The mixture solution was stirred overnight at 70°C. The active layer was prepared in glove-box by spinning the P3HT:$PC_{61}BM$ solution onto the glass/ITO/PEDOT:PSS, glass/HC-PEDOT:PSS or glass/SF/HC-PEDOT:PSS substrates. The wet films were slowly dried and then annealed at 110°C for 10 minutes, resulting in ~ 350 nm thick films. Thinner active blends, used to better evaluate the effect of the LDS layer, were obtained by preparing a P3HT:$PC_{61}BM$ solution with a total concentration of 20 mg/ml and by spinning it onto the glass/SF/HC-PEDOT:PSS or glass/Stb:SF/HC-PEDOT:PSS. The wet films were then annealed at 110°C for 10 minutes, resulting in ~ 100 nm thick films.
To complete the device fabrication, LiF and Al (0.6 nm and 100 nm, respectively) were deposited sequentially without breaking vacuum (~ 1×10^{-6} Torr) using a thermal evaporator directly connected to the glove box. The current–voltage (I–V) characteristics of all OPV devices were recorded by a Keithley 236 source-measure unit under simulated AM1.5G illumination of 100 mW/cm^2 (Abet Technologies Sun 2000 Solar Simulator). The light intensity was determined by a calibrated silicon solar cell fitted with a KG5 color glass filter to bring spectral mismatch to unity. The active area of the solar cell was exactly 6 mm^2. During testing, each cell was carefully masked, by calibrated mask, to prevent an excess photocurrent generated from the parasitic device regions outside the overlapped electrodes area. All I–V measurements were performed inside the glove box in oxygen and moisture free environment. The spectral response, or External Quantum Efficiency (EQE), of the devices was measured with a home built system on encapsulated devices; monochromatic light was obtained with a Xenon arc lamp from Lot-Oriel (300 Watt power) coupled with a Spectra-Pro monochromator; the monochromatic light was pulsed by means of an optical chopper (~ 500 Hz frequency) and collected with a Lock-In Digital Amplifier SR830; a calibrated UV-enhanced Silicon photodiode was used as reference; the experimental error was ~ 10% for each point (for each wavelength).

2.5 Thin-film characterization

All thin-film characterizations were performed in air. Transmittance and absorption UV-vis spectra were recorded on a JASCO V-550 spectrophotometer. The thickness of the various films was measured by a profilometer (KLA Tencor, P-6). Atomic Force Microscopy (AFM) images were taken with a Solver Pro (NT-934 MDT) scanning probe microscope in tapping mode. The Mid IR (400-4000 cm^{-1}) absorption measurements, performed on silk films spin-coated onto high resistivity silicon substrates, were recorded with a Bruker IFS-113v FTIR interferometer at 4 cm^{-1} resolution averaging over 512 scans in order to improve the signal to noise ratio. The emission spectra were measured by irradiating the samples with a He-Cd laser (Kimmon Koha) and detecting in transmission conditions the emitted light by an optical multichannel analyzer (Hamamatzu Photonics). The photoluminescence quantum efficiency was calculated with a fluorimeter equipped with an integrating sphere (Hamamatsu Photonics). Confocal laser scanning microscopy imaging was carried out by using a Nikon TE2000 optical microscope connected with a Nikon EZ-1 confocal scanning head.

Results and discussion

3.1 Pristine SF film: preparation and characterization

SF films were prepared on glass or silicon substrates by spin coating SF water solutions, obtaining ~ 400 nm thin films. The first step of our study was to investigate the chemical-physical properties of the SF films and tailor them for the integration of SF into ITO-free BHJ solar cells. Indeed, some fundamental features are demanded to SF films to be used as effective and inert substrate for OPV devices: i) water insolubility, to allow the subsequent deposition of the water based solution of HC-PEDOT:PSS (polymeric anode), ii) film surface homogeneity and smoothness, to favour the subsequent deposition and thus the quality of overlying layers, and iii) optical transparency.
The above mentioned physical properties of SF films depend on the conformation of the fibroin protein structure in the solid state. In particular, a random coils and α helixes organization (silk I) leads to water soluble and transparent films, while more organized and hydrophobic β-sheet domains (silk II) confer water insolubility together with an increased opacity [19]. For our purposes, a compromise between the silk I and silk II content in the SF film should be found. This can be done by applying several post-deposition treatments [20], such as water annealing, exposition to organic solvents, mechanical stress [8a,21]. Here, the silk I/silk II phase ratio was controlled through a pre-deposition technique, by doping the pristine SF solution with 2.5% (v/v) of DMSO as processing solvent additive, with an approach already tested for SF sponges [22].
IR spectroscopy on pristine SF films and DMSO-doped SF films was carried out to determine the effect of the treatment on the random coil and β-sheet content (Figure 1A) [23].

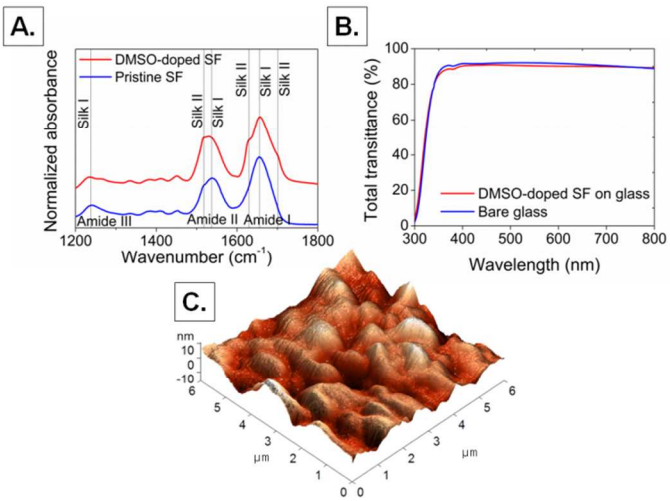

Figure 1. A) FTIR spectrum of pristine (blue) and DMSO doped (red) SF film spun cast on silicon substrate; **B**) Total transmittance spectrum of bare glass (blue) and ~ 400 nm thick DMSO doped SF film spin coated on glass substrate (red); **C**) Tapping mode AFM (3D) image (size: 6 μm × 6 μm) of DMSO doped SF film deposited by spin coating on glass substrate (RMS ~ 3.5 nm).

The typical absorption bands of amide I (C=O stretching), amide II (N-H deformation and C-N stretching) and those of amide III (C-N stretching and N-H deformation) lie approximately at 1650, 1530 and 1250 cm^{-1} for a random coil (or silk I) structure and at 1630, 1520 and 1230 cm^{-1} for a β-sheet (or silk II) conformation, respectively [24]. In the doped SF film, together with the bands commonly assigned to the silk I structure (1655, 1535 and 1240 cm^{-1}), new bands at 1621, 1517 and 1232 cm^{-1}, characteristics of silk II conformation, appear, confirming the effectiveness of the involved method.

We next tested the water resistance of DMSO-doped SF films by soaking them in acidic water (pH = 2) for 60 seconds, to simulate the conditions of the subsequent deposition of HC-PEDOT:PSS. Of note, no significant change in terms of film thickness, optical transparency and surface roughness was observed (experimental data and additional details are reported in the Supporting Information in Table S1, Figures S1 and S2).

The transparency of the resulting water insoluble films was tested by measuring the total transmittance spectrum of a DMSO-doped SF film deposited on glass (Figure 1B). A high optical transmittance (~ 90%) over the entire visible range, nearly identical to the reference glass substrate, was observed.

Finally, morphological investigations on insoluble SF films were carried out by tapping-mode AFM analysis (Figure 1C). A relatively smooth and regular surface, with a low surface roughness (RMS ~ 3.5 nm), was observed for the DMSO-doped SF films, similarly to what was found for analogous water insoluble SF films obtained with a methanol post-deposition treatment (RMS ~ 4.0 nm) [25]. The SF films obtained with the described method are then suitable for being integrated as bottom layers for ITO-free organic solar cells.

3.2 OPV device fabrication and characterization

ITO-free bulk heterojunction (BHJ) solar cells were prepared on the top of the SF water insoluble films. The device structure employed, glass/SF/HC-PEDOT:PSS/P3HT:PC61BM/LiF/Al, is depicted in Figure 2A (additional details for device fabrication are reported in the Experimental Section).

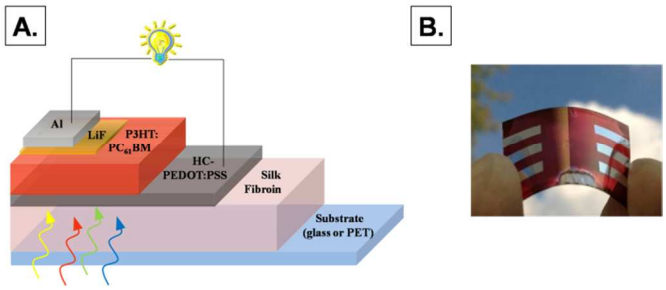

Figure 2. Device structure of the silk fibroin-based ITO-free BHJ solar cell (**A**) and picture of the relative device fabricated on PET substrate (**B**).

The first step for the fabrication of the device was the deposition of the polymeric semi-transparent electrode (HC-PEDOT:PSS) onto the glass/SF substrate. The UV-ozone treatment usually employed to deposit PEDOT:PSS over ITO or glass to improve the substrate affinity would be detrimental in the case of the SF film. To overcome this issue, a low volume (1% v/v) of surfactant (Triton X-100) was added to the HC-PEDOT:PSS solution. A homogeneous and smooth HC-PEDOT:PSS layer was obtained, as confirmed by AFM measures (Figure S3). The optimal thickness of the HC-PEDOT:PSS layer, tested in complete devices, was found to be 120 nm, resulting the best compromise between electrical conductivity and optical transparency [26]. Note that the thermal annealing of the HC-PEDOT:PSS layer (120°C for 20 minutes) did not alter the optical and/or morphological properties of the underlying SF film, as reported in Table S1, Figures S1 and S2.

The OPV device fabrication was completed by active layer and cathode deposition on the optimized HC-PEDOT:PSS layer, as described in the Experimental section. ITO-free solar cells on bare glass and common ITO-based devices were also fabricated as reference systems and their photovoltaic performance was compared with that of SF-integrating solar cells. For clarity, the device structure fabricated and analyzed are reported below:

Device A (ITO-based solar cell):
glass/ITO/PEDOT:PSS/P3HT:PC61BM/LiF/Al
Device B (ITO-free solar cell):
glass/HC-PEDOT:PSS/P3HT:PC61BM/LiF/Al
Device C (SF-based ITO-free solar cell):
glass/SF/HC-PEDOT:PSS/P3HT:PC61BM/LiF/Al

Table 1 summarizes the OPV response data of the solar cells, including open-circuit voltage (V_{OC}), short-circuit current density (J_{SC}), fill factor (FF) and power conversion efficiency (PCE). The corresponding current density-voltage (J−V) curves, under standard illumination, are shown in Figure 3.

Table 1. OPV performance of P3HT:$PC_{61}BM$ based solar cells using different device structures. The reported data are averaged over 5 devices.

OPV device structure	J_{SC} [mA/cm^2]	V_{OC} [V]	FF [%]	PCE [%]
Device A	8.5	0.56	63	3.0
Device B	7.7	0.56	64	2.8
Device C	7.7	0.56	59	2.6

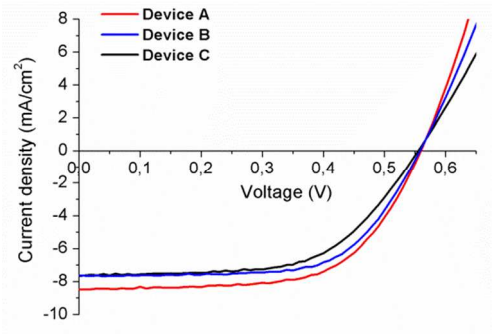

Figure 3. *J-V* plot, under standard illumination, of BHJ solar cells employing the following structures: glass/ITO/PEDOT:PSS/P3HT:$PC_{61}BM$/LiF/Al (Device A – red trace), glass/HC-PEDOT:PSS/P3HT:$PC_{61}BM$/LiF/Al (Device B – blue trace) and glass/SF/HC-PEDOT:PSS/P3HT:$PC_{61}BM$/LiF/Al (Device C – black trace).

As expected, ITO-free solar cells (device B and C) exhibit a slightly lower PCE with respect to the ITO-based reference (device A) due to a slight decrease in J_{SC} (Table 1). This is due to the reduced optical transparency of the anode (a thick layer of HC-PEDOT:PSS for devices B and C comparing to a thin layer of PEDOT:PSS on ITO for device A) [17].

Interestingly, the SF-based solar cells (device C) displayed a photovoltaic performance comparable to that of the ITO-free reference systems (device B). Of note, identical J_{SC} (7.7 mA/cm^2) confirms the high optical transparency of the SF film, which clearly does not influence the light harvesting and charge generation of the active layer. The small difference in PCE can be mainly ascribed to the reduction in FF (64% vs 59%, respectively for device B and C) passing from ITO-free to SF-based devices. This variation can be explained by the slightly higher RMS of the SF film with respect to the glass substrate (RMS < 1 nm), which partially influences the nanomorphology and thus the charge transport properties of the overlying polymeric electrode (HC-PEDOT:PSS).

In order to use the SF film as a LDS layer, we doped the SF layer with a commercial water soluble derivative of stilbene (Stb). A homogeneous dispersion of Stb in the SF matrix was obtained (Figure S4). The spectral features of the dye were maintained in the SF matrix (Figure 4 and Figure S5), together with its high emission QY (~ 60%, Table S2).

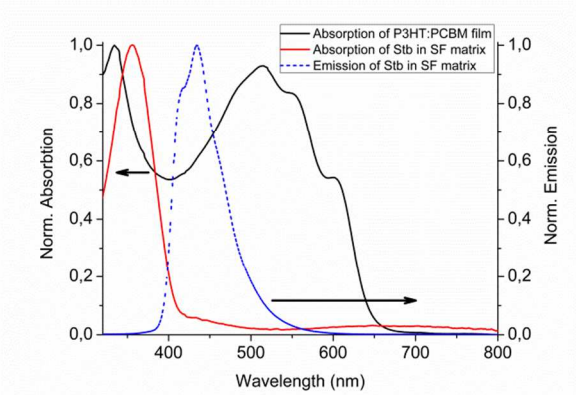

Figure 4. Normalized absorption (red) and emission (dashed blue line) spectra of Stb dye in SF matrix compared to the absorption spectrum of P3HT:$PC_{61}BM$ blend film (black).

In addition, by observing the FT-IR spectrum of the Stb:SF layer compared to bare SF, an enhancement of the β-sheet conformation of the SF polymeric chains was evidenced (Figure S6). Nevertheless, desirably, the enhanced β-sheet conformation did not lead to a decrease of the film total transmittance in the 420 – 700 nm wavelength region (~ 90%, Figure S7), where the main absorption band of the P3HT:PC61BM active layer lies.

In sight of these results, Stb should represent a promising dye for the reported application.

To evaluate the suitability of the Stb:SF films as LDS layers, the normalized absorption and emission spectra of the optimized Stb:SF film together with the absorption spectrum of the P3HT:$PC_{61}BM$ active layer were compared (Figure 4).

It should be noted that the spectral match between Stb and P3HT:$PC_{61}BM$ is not optimal, since there is a significant overlap between the active layer and the dye absorption spectra, while the Stb emission maximum (435 nm) does not match the absorption maximum of P3HT (515 nm). In particular, the partial overlap between the absorption spectra of the LDS and the P3HT:$PC_{61}BM$ layers can cause a decrease of the excitons produced in the active layer by means of direct absorption of the incident photons in that spectral region. Due to these sub-optimal conditions, to obtain an overall enhancement of the total charges generated in the device, a good balance between the absorbance of the LDS layer and that of the active layer is required. To this aim, devices with both standard (~ 350 nm) and thin (~ 100 nm) active layers were tested, while different Stb concentrations were studied.

The amount of Stb to be dispersed in SF films was optimized by measuring the emission spectra of Stb:SF films with Stb concentrations ranging from 3 to 7 wt %. The maximum emission intensity was obtained for the LDS layer with 5 wt % of Stb (Figure S5).

The optimized Stb:SF film was then integrated as LDS layer into ITO-free solar cells, obtaining devices with the structure reported below (device D):

Device D (Stb:SF-based ITO-free solar cell):

glass/Stb:SF/HC-PEDOT:PSS/P3HT:PC_{61}BM/LiF/Al

A first comparison between the photovoltaic performance of devices with structure C (SF-based ITO-free solar cell) and D (Stb:SF-based ITO-free solar cell), with both thick and thin P3HT:PC_{61}BM active layers, did not reveal any improvement due to the presence of the LDS layer (Table S4).
However, for a deeper analysis, the spectral response (or EQE) of devices C and D was measured. The EQE spectrum is the ratio, at each wavelength, between the number of electrons extracted from the cell and the number of incident photons at that wavelength. In our experiment, any change in the EQE spectra due to the presence of the LDS layer should be observed in the absorption range between 300 and 400 nm, where incident photons produce charges by the direct absorption of the active layer or by absorption/emission of the LDS and re-absorption of the active layer. The EQE spectra of devices C and D are reported in Figure 5.

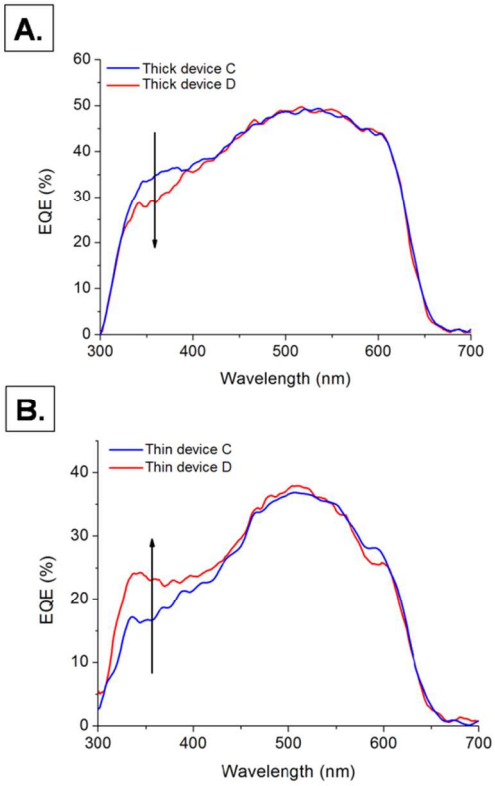

Figure 5. EQE spectra of SF-based (blue) and Stb:SF-based (red) devices with thick (A) and thin (B) active layer of P3HT:PC_{61}BM. The black arrow, placed at the wavelength corresponding to the maximum absorbance of Stb, evidences the effect of the introduction of the LDS.

The EQE spectrum of thick device D compared to thick device C (Figure 5A) showed a lowering between 300 and 400 nm. This means that, in the case of thicker active layers, the number of charges generated by P3HT:PC_{61}BM from the direct absorption of incident photons in the 300-400 nm range is higher than that produced from the photons converted by the LDS. In other words, the LDS produces a "shadow effect" between 300 and 400 nm that is not fully compensated by the photons emitted at longer wavelength and re-absorbed by the active layer. On the other hand, by comparing the EQE spectrum of thin device D with thin device C (Figure 5B), an evident increase in the spectral response between 300 and 400 nm was detected. Therefore, in this case, the contribution of the LDS layer overcomes the cited "shadow effect".
From the observed increase in the spectral response of the thin devices with the LDS layer an increase in photocurrent was calculated by convoluting the EQE spectra over the solar radiation spectrum. For the thin devices, the calculated J_{SC} is 4.80 mA/cm^2 and 5.00 mA/cm^2 respectively for devices C and D, resulting in a J_{SC} variation of 4%. Note that the LDS layer, even though causing evident changes in the intensity/shape of the EQE spectra between 300 and 400 nm, produces such a low J_{SC} enhancement due to the low photon flux of the solar radiation in that spectral range. For this reason the LDS effect was not observable in the J-V curves registration, being the J_{SC} enhancement comparable to the experimental error of the measurement (5%).
Our experiments clearly demonstrate the suitability of the bio-derived SF films to act as functional bottom layer in organic solar cells. Possibly, better performing silk-based LDS layers can be obtained through a finer engineering of the device, i.e.: i) the use of semiconducting donor polymers different from P3HT, which allow the fabrication of optimized devices with thinner active layers [27]; ii) the choice of the donor polymer and luminescent dye couple having a higher overlap between their respective absorption and emission spectra, together with a lower overlap between their absorption spectra; iii) the use of thicker SF films prepared with techniques different from spin coating, [28] allowing a higher load of luminescent doping molecules to be embedded in the SF matrix and enhancing the total absorption and emission of the resulting LDS layer.
Furthermore, we analyzed the chemical-physical stability and shelf life of the silk-integrated solar cells along a period of 70 days inside a glove box at room temperature (in ambient lighting conditions). The temporal evolution of the photovoltaic parameters of the prepared devices (A, B, C and D) are reported as percentage variations over time in Figure 6 (only PCE) and as percentage variations after 70 days in Table 2 (all parameters).

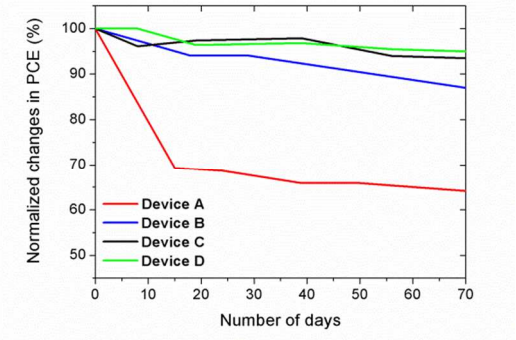

Figure 6. Percentage variation of PCE of devices A, B, C and D along 70 days.

Table 2. Percentage variation of the photovoltaic parameters of different device structures (A, B,C and D) after 70 days. The reported data are averaged over 5 devices.

OPV device	Reduction of J_{SC}	Reduction of V_{OC}	Reduction of FF	Reduction of PCE
Device A	25 %	4 %	5 %	36 %
Device B	10 %	4 %	3 %	13 %
Device C	0 %	4 %	4 %	6 %
Device D	0 %	4 %	2 %	5 %

Despite the slight decrease of V_{OC} and FF common to all devices, the J_{SC} variation is the main parameter influencing the PCE trend over time (Table 2). All ITO-free devices (B, C and D) resulted more stable comparing to the ITO-based reference (A), which degraded faster due to the detrimental chemical interactions occurring at the PEDOT:PSS/ITO interface, as known from literature [29]. Interestingly, within the ITO-free solar cells, the devices with bare and Stb-doped SF films (devices C and D) resulted much more stable compared to the analogous ITO-free devices (B), with a reduction of PCE of only 6% after 70 days. We can suppose that the SF layer improves the HC-PEDOT:PSS electrode stability over time, probably by generating some interfacial interactions which partially hinder further rearrangements of the polymeric chains. Finally, the potential of SF films as free-standing and flexible support material for OPVs was tested. Flexible SF-based solar cells fabricated on PET (polyethylene terephthalate) (Figure 2B) showed a photovoltaic performance comparable to their references (flexible ITO-free devices), as shown in Table S3 and Figure S8. Moreover, the mechanical properties of the SF layer for flexible OPV devices applications were verified by means of simple bending tests. Interestingly, the SF-based device on PET showed nearly constant OPV performance after several bending cycles with a bending radius of 10 mm (Figure S9).

Conclusions

Our results clearly show that efficient and stable silk-integrated ITO-free BHJ solar cells can be fabricated. The experimental challenges of preparing transparent, homogeneous, water-stable and PEDOT:PSS-affine SF films were solved by the accurate study of the film processing conditions. The possibility to dope the SF film with luminescent molecules and use it as LDS layer in the OPV was demonstrated. Considering our results and the remarkable properties of doped SF films and composites [9,12], challenging but promising opportunities are offered by the integration of multifunctional SF films in OPV devices, to enhance their performances and to promote a sustainable OPV technology. Moreover, the ability of the silk-integrated OPV devices prepared on PET to preserve their photovoltaic performances after several bending cycles proves the possibility to obtain devices on free-standing flexible SF films. In conclusion, this work validates the potential of SF as natural biopolymer for the development of a next generation of low cost, fully printable, efficient and "green" OPV devices. To note, in light of the recent demonstration of the use of the OPV principle in the neuroprosthetics as artificial retina, our results on the use of biocompatible SF in flexible, transparent and performing OPV device could open the way for a plethora of applications also in the biomedical field [30].

Acknowledgements

The work was financially supported by Progetto Bandiera Fabbrica del Futuro, Silk.it (V.B, A.S.) and MIUR through Futuro in Ricerca RBFR12SJA8 (V.B), Consorzio MIST E-R through Programma Operativo FESR 2007-2013 della Regione Emilia-Romagna – Attività I.1.1", and EU through project FP7-PEOPLE-2012-ITN 316832-OLIMPIA. The authors wish to thank Vincenzo Ragona for the technical support.

Notes and references

[a] Consiglio Nazionale delle Ricerche (CNR) – Istituto per lo Studio dei Materiali Nanostrutturati (ISMN), Via P. Gobetti, 101, 40129, Bologna, Italy.
[b] Consiglio Nazionale delle Ricerche (CNR) - Istituto per la Sintesi Organica e la Fotoreattività (ISOF), Via P. Gobetti, 101, 40129, Bologna, Italy. E-mail: mirko.seri@isof.cnr.it, valentina.benfenati@isof.cnr.it, Tel: +39 0516399771, +39 0516399786; Fax: +39 0516399844.
[c] Laboratory MIST E-R, Via P. Gobetti, 101, 40129, Bologna, Italy.

Electronic Supplementary Information (ESI) available: solubility tests, thermal tests, transmittance spectra, AFM images of DMSO doped SF films; confocal fluorescence images, absorption and emission spectra, photoluminescence QY, FT IR spectra, transmittance spectra of STB:SF films; J-V plots of flexible devices and of thick and thin devices. See DOI: 10.1039/b000000x/

1 a) R. R. Sondergaard, M. Hosel and F. C. Krebs, *J. Polym. Sci., Part B: Polym. Phys.*, 2013, **51**, 16-34; b) C. J. Brabec, *Sol. Energ. Mat. Sol. Cells*, 2004, **83**, 273-292; c) M. Jorgensen, J. E. Carlè, R. R. Sonderggard, M. Lauritzen, N. A. Dagnaes-Hansen, S. L. Byskov, T. R. Andresen, T. T. Larsen-Olsen, A. P. L. Bottiger, B. Andreasen, L. Fu, L. Zuo, Y. Liu, E. Bundgaard, X. Zhan, H. Chen and F.C. Krebs, *Sol. Energ. Mat. Sol. Cells*, 2013, **119**, 84-93; d) D. M. de Leeuw and E. Cantatore, *Mater. Sci. Semicond. Process*., 2008, **11**, 199-204.
2 a) L. Rigamonti, M. Grosso, J. Moller, V. Martinez Sanchez, S. Magnani and T.H. Christensen, *Resour. Conserv. Recy*., 2014, **85**, 42-53; b) J. Groot, X. Bing, H. Bos-Brouwers and J. Bloemhof-Ruwaard, *Resour. Conserv. Recy*., 2014, **85**, 79-87.
3 a) M. Irimia-Vladu, *Chem. Soc. Rev*., 2014, **43**, 588; b) S.-W. Hwang, J.-K. Song, X. Huang, H. Cheng, S.-K. Kang, B. H. Kim, J.-H. Kim, S. Yu, Y. Huang and J. A. Rogers, *Adv. Mater*., 2014, **26**, 3905-3911.
4 a) Y. Zhou, C. Fuentes-Hernandez, T. M. Khan, J. C. Liu, J. Hsu, J. W. Shim, A. Dindar, J. P. Youngblood, R. J. Moon and B. Kippelen, *Sci. Rep.*, 2013, **3**, 1536; b) S. Ummartyotin, J. Juntaro, M. Sain and H. Manuspiya, *Ind. Crop. Prod.*, 2012, **35**, 92-97.
5 M. Strange, D. Plackett, M. Kaasgaard and F.C. Krebs, *Sol. Energ. Mat. Sol. Cells*, 2008, **92**, 805-813.

6 M. Irimia-Vladu, P. A. Troshin, M. Reisinger, L. Shmygleva, Y. Kanbur, G. Schwabegger, M. Bodea, R. Schwodiauer, A. Mumyatov, J. W. Fergus, V. F. Razumov, H. Sitter, N. S. Sariciftci and S. Bauer, *Adv. Funct. Mater*., 2010, **20**, 4069-4076.

7 a) F. Omenetto and D. L. Kaplan, *Science*, 2010, **329**, 528-531 ; b) R. Capelli, J. J. Amsden, G. Generali, S. Toffanin, V. Benfenati, M. Muccini, D.L. Kaplan, F.G. Omenetto and R. Zamboni, *Org. Electron.*, 2011, **12**, 1146-1151; c) C. B. Borkner, M. B. Elsner and T. Scheibel, *ACS Appl. Mater. Interfaces*, 2014 dx.doi.org/10.1021/am5008479.

8 a) H-J. Jin and D. J. Kaplan, *Nature*, 2003, **424**, 1057-1061; b) O. Shchepelina, I. Drachuk, M. K. Gupta, J. Lin and V. V. Tsukruk, *Adv. Mater*., 2011, **23**, 4655-4660; c) L. F. Drummy, D. M. Phillips, M. O. Stone, B. L. Farmer and R. R. Naik, *Biomacromolecules*, 2005, **6**, 3328-3333; d) R. Nazarov, H.J. Jin and D.L. Kaplan, *Biomacromolecules*, 2004, **5**, 718-726.

9 a) T. Posati, V. Benfenati, A. Sagnella, A. Pistone, M. Nocchetti, A. Donnadio, G. Ruani, R. Zamboni and M. Muccini, *Biomacromolecules*, 2014, **15**, 158-168; b) G. Ruani, A. Sagnella, C. Chieco, N. Di Virgilio, S. Toffanin, T. Posati, A. Pistone, S. Bonetti, M. Muccini, V. Benfenati, F. Rossi and R. Zamboni, *RSC Advances*, 2014, DOI: 10.1039/c4ra04622f

10 a) J. J. Amsden, H. Perry, V. S. Boriskina, A. Gopinath, D. L. Kaplan, L. Dal Negro and F. G. Omenetto, *Opt. Express*, 2009, **17**, 21271- 21279; b) S. Kim, A. N. Mitropoulos, J. D. Spitzberg, H. Tao, D. L. Kaplan and F. G. Omenetto, *Nat. Photonics*, 2012, **6**, 818-823; c) K. Tsioris, H. Tao, M. Liu, J. A. Hopwood, D. L. Kaplan, R. D. Averitt and F. G. Omenetto, *Adv. Mater*., 2011, **23**, 2015-2019; d) C. J. Bettinger, K. M. Cyr, A. Matsumoto, R. Langer, J. T. Borenstein and D. L. Kaplan, *Adv. Mater*., 2007, **19**, 2847-2850.

11 a) D. Kim, Y. Kim, J. Amsden, B. Panilaitis, D. L. Kaplan, F. G. Omenetto, M. R. Zakin and J. A. Rogers, *Appl. Phys. Lett*., 2009, **95**, 133701; b) D.-H. Kim. J. Viventi, J. J. Amsden, J. Xiao, L. Vigeland, Y.-S. Kim, J. A. Blanco, B. Panilaitis, E. S. Frechette, D. Contreras, D. L. Kaplan, F. G. Omenetto, Y. Huang, K.-C. Hwang, M. R. Zakin, B. Litt and J. A. Rogers, *Nat. Mater*., 2010, **9**, 511-517.

12 a) M. Melucci, M. Durso, L. Favaretto, M. L. Capobianco, V. Benfenati, A. Sagnella, G. Ruani, M. Muccini, R. Zamboni, V. Fattori and N. Camaioni, *RSC Adv*., 2012, **2**, 8610-8613; b) S. Toffanin, S. Kim, S. Cavallini, M. Natali, V. Benfenati, J. J. Amsden, D. L. Kaplan, R. Zamboni, M. Muccini and F. G. Omenetto, *Appl. Phys. Lett*., 2012, **101**, 091110; c) E. M. Pritchard, P. B. Dennis, F. Omenetto, R. R. Naik and D. L. Kaplan, *Biopolymers*, 2012, **97**, 479-498.

13 a) C. J. M. Emmott, A. Urbina and J. Nelson, *Sol. Energ. Mat. Sol. Cells*, 2012, **97**, 14-21; b) R. Po, C. Carbonera, A. Bernardi, F. Tinti and N. Camaioni, *Sol. Energ. Mat. Sol. Cells*, 2012, **100**, 97-114.

14 a) E. Klampaftis, D. Ross, K. R. McIntosh and B. S. Richards, *Sol. Energ. Mat. Sol. Cells*, 2009, **93**, 1182–1194; b) G. F. Ma, H.-J. Xie, P.-P. Cheng, Y.-Q. Li and J.-X. Tang, *Appl. Phys. Lett*., 2013, **103**, 043302.

15 J. L. Charlton and J. Saltiel, *J. Phys. Chem*., 1977, **81**, 1940–1944.

16 V. Benfenati, K. Stahl, C. Gomis-Perez, S. Toffanin, A. Sagnella, R. Torp, D. L. Kaplan, G. Ruani, F. G. Omenetto, R. Zamboni and M. Muccini, *Adv. Funct. Mater*., 2012, **22**, 1871-1884.

17 O. P. Dimitriev, D. A. Grinko, Y. V. Noskov, N. A. Ogurtsov and A. A. Pud, *Synthetic Met*., 2009, **159**, 2237-2239.

18 M. Vosgueritchian, D. J. Lipomi and Z. Bao, *Adv. Funct. Mater*., 2012, **22**, 421-428.

19 a) X. Hu, D.L. Kaplan and P. Cebe, *Macromolecules*, 2008, **41,** 3939-3948; b) X.-G. Li, L.-Y. Wu, M.-R. Huang, H.-L. Shao and X. H. Hu, *Biopolymers*, 2008, **89,** 497-505.

20 B.D. Lawrence, F. Omenetto, K. Chiu and D.L. Kaplan, *J. Mater. Sci*., 2008, **43**, 6967-6985.

21 a) X. Hu, D. Kaplan and P. Cebe, *Thermochim. Acta*, 2007, **461**, 137-144; b) M. Ishida, T. Asakura, M. Yokoi and H. Saito, *Macromolecules*, 1990, **23**, 88-94.

22 Y. Tamada, *Biomacromolecules*, 2005, **6**, 3100-3106.

23 T. Miyazawa and E.R. Blout, *J. Am. Chem. Soc*., 1961, **83**, 712-719.

24 K. Yamada, Y. Tsunoi and A. Itaya, *Thin Solid Films*, 2003, **440**, 208-216.

25 E. Servoli, D. Maniglio, A. Motta, R. Predazzer and C. Migliaresi, *Macromol. Biosci*., 2005, **5**, 1175-1183.

26 a) S. Na, S. Kim, J. Jo and D. Kim, *Adv. Mater*., 2008, **20**, 4061-4067; b) D. J. Lipomi, B. C. K. Tee, M. Vosgueritchian and Z. Bao, *Adv. Mater*., 2011, **23**, 1771-1775; c) D. Angmo and F. C. Krebs, J. *Appl. Polym. Sci*., 2013, **129**, 1-14; d) M. W. Rowell, M. A. Topinka, M. D. McGehee, H. J. Prall, G. Dennler, N. S. Sariciftci, L. Hu and G. Gruner, *Appl. Phys. Lett*., 2006, **88**, 233506; e) L. G. De Arco, Y. Zhang, C. W. Schlenker, K. Ryu, M. E. Thompson and C. Zhou, *ACS Nano*, 2010, **4**, 2865-2873.

27 a) A. Abbotto, M. Seri, M. S. Dangate, F. De Angelis, N. Manfredi, E. Mosconi, M. Bolognesi, R. Ruffo, M. M. Salamone, and M. Muccini, *J. Polym. Sci. A Polym. Chem*., 2012, **50**, 2829–2840; b) M. Seri, M. Bolognesi, Z. Chen, S. Lu, W. Koopman , A. Facchetti, and M. Muccini, *Macromolecules*, 2013, **46**, 6419–6430; c) M. Bolognesi, D. Gedefaw, D.Dang, P. Henriksson, W. Zhuang, M. Tessarolo, E. Wang, M. Muccini, M. Seri and M. R. Andersson, *RSC Advances*, 2013, **46**, 24543-24552; d) W. Zhuang, M. Bolognesi, M. Seri, P. Henriksson, D. Gedefaw, R. Kroon, M. Jarvid, A. Lundin, E. Wang, M. Muccini and M. R. Andersson, *Macromolecules*, 2013, **46**, 8488–8499; e) D. Gedefaw, M. Tessarolo, W. Zhuang, R. Kroon, E. Wang, M. Bolognesi, M. Seri, M. Muccini and M. R. Andersson, *Polymer Chemistry*, 2014, **5**, 2083-2093; f) M. Tessarolo, D. Gedefaw, M. Bolognesi, F. Liscio, P. Henriksson, W. Zhuang, S. Milita, M. Muccini, E. Wang, M. Seri and M. R. Andersson, *J. Mater. Chem. A*, 2014, **2**, 11162-11170.

28 X. Wang, H. J. Kim, P. Xu, A. Matsumoto and D. L. Kaplan, *Langmuir*, 2005, **21**, 11335-11341.

29 M. Girtan and M. Rusu, *Sol. Energ. Mat. Sol. Cells*, 2010, **94**, 446-450.

30 a) V. Gautam, D. Rand, Y. Hanein and K. S. Narayan, *Adv. Mater*, 2014, **26**, 1751-1756; b) D. Ghezzi, M. R. Antognazza, R. Maccarone, S. Bellani, E. Lanzarini, N. Martino, M. Mete, G. Pertile, S. Bisti, G. Lanzani and F. Benfenati, *Nat. Photonics*, 2013, **7**, 400; c) V. Benfenati, N. Martino, M. R. Antognazza, A. Pistone, S. Toffanin, S. Ferroni, G. Lanzani and M. Muccini, *Adv. Healthc. Mater*., 2014, **3**, 392-9.

